frontiers | Frontiers in Energy Research

TYPE Original Research
PUBLISHED 06 April 2023
DOI 10.3389/fenrg.2023.1177437

OPEN ACCESS

EDITED BY
Yongfei Yang,
Nantong University, China

REVIEWED BY
Bing Qi,
Lanzhou University of Technology, China
Yonghai Yu,
Hohai University, China
Banglun Zhou,
Guizhou Institute of Technology, China

*CORRESPONDENCE
Mengcheng Wang,
jdwmc2018@163.com

SPECIALTY SECTION
This article was submitted to Process and Energy Systems Engineering, a section of the journal Frontiers in Energy Research

RECEIVED 01 March 2023
ACCEPTED 22 March 2023
PUBLISHED 06 April 2023

CITATION
Chen J, Wang M, Bao Y, Chen X and Xia H (2023), Mixed-flow pump performance improvement based on circulation method.
Front. Energy Res. 11:1177437.
doi: 10.3389/fenrg.2023.1177437

Mixed-flow pump performance improvement based on circulation method

Jiaqi Chen[1], Mengcheng Wang[2]*, Yonghao Bao[2], Xiao Chen[3] and Hepeng Xia[4]

[1]National Research Center of Pumps, Jiangsu University, Zhenjiang, China, [2]College of Electrical, Energy and Power Engineering, Yangzhou University, Yangzhou, China, [3]Anhui Ding Yuan Engineering Construction Co., Hefei, China, [4]Jiangsu Province Water Engineering Sci-tech Consulting Co., Nanjing, China

Mixed-flow pumps have been extensively employed in daily life, improving their energy characteristics contribute to the reduction of energy consumption worldwide. In this study, to overcome the decrease of optimization upper limit caused by using a single type of parameter as the design parameter, a typical mixed-flow pump was chosen for study, and its impeller was parameterized by five geometric and eight hydrodynamic parameters. With head and efficiency as the constraint and optimization objective respectively, 27 schemes were constructed by the Taguchi method. The influence of design factors to the objective and constraint was analyzed based on range and regression analysis. The optimization mechanism was elucidated using the entropy production method. The result reveals that the geometric and hydrodynamic parameters have a significantly impact on the mixed-flow pump's energy characteristics. The optimized model head is 12.43m, which meets the constraints, while the efficiency increases by 3.2%–88.51%. Therefore, considering both geometric and hydrodynamic parameters in the mixed-flow pump optimization is workable and necessary. This paper can provide practical instructions on the optimal design of different turbomachines.

KEYWORDS

pump, coupling optimization, circulation method, geometric and hydrodynamic parameters, numerical simulation

1 Introduction

As a general-purpose machine, pumps have been extensively employed in daily life, especially mixed-flow pumps with moderate head and large flow rates, which are highly sought after (Kim et al., 2019; Wang et al., 2021a). However, the energy consumption of pumps is also staggering, with recent studies showing that their share of total energy consumption exceeds 22%, and is set to increase further to over 30% in the next decade (Gu et al., 2022a). Hence, improving the energy conversion efficiency of mixed-flow pumps is very important.

Among the many in-depth studies on turbomachinery design optimization, Zangeneh (1991) creatively proposed the circulation method, which uses hydrodynamic parameters (circulation, pressure and loading, etc) as design parameters in the blade parameterization. The greatest advantage of the circulation method is the close connection between parameters and hydraulic performance (Lu et al., 2018; Zhang and Zhao, 2020), as well as easier access to innovative solutions (Yin and Wang, 2014; Fallah-Ardeshir et al., 2020). More importantly,

the design results obtained by the circulation method represents the optimal flow field distribution rather than the best combination of geometric parameters, which can provide designers with more valuable references in future optimization studies (Leguizamon and Avellan, 2020; Gu et al., 2022b).

The effectiveness of the circulation method was extensively demonstrated in previous study. Zangeneh et al. (1996) successfully suppressed the secondary flow within a mixed flow pump using the circulation method in an optimization study. In subsequent work, Goto et al., 1996) verified the validity of this work through experiments. Huang et al. (2015) using blade loading as design parameters carried out a parametric optimization for the impeller of a mixed-flow pump, and found that changing the position of the first loading point can effectively inhibit the blade suction surface flow separation. Bonaiuti et al. (2010) investigated the effectiveness of the circulation method in mixed-flow water-jet pumps by varying impeller outlet circulation distribution. They found that the hydraulic mixing losses near the diffuser outlet and the secondary flow losses in the diffuser can be effectively balanced by adjusting the value of the diffuser outlet residual circulation. In another study (Bonaiuti and Zangeneh, 2009), they investigated the compressor diffuser and impeller coupling optimization by changing the loading pattern at the hub and shroud. Ma et al. (2019) performed a performance improvement for a turbine runner by circulation method, and investigated the effect of several key hydrodynamic factors on the Francis turbine runner by model comparison. Yang and Xiao (2014) conducted a similar study on a Pump-Turbine impeller and successfully improved the model's efficiency in both turbine and pump mode. Lee et al. (2008) optimized an axial fan using the Taguchi method with blade leading edge loading and loading pattern as design parameters. According to the idea of Taguchi's method, Yang et al. (2017) investigated the impact of loading distribution to a submersible axial flow pump. Wang et al. (2022) compared the advantages and disadvantages of three different circulation distributions in mixed-flow pump design optimization by coupling Taguchi and circulation method.

An obvious similarity between the above studies is that only hydrodynamic parameters were used as design parameters. However, some studies have shown that geometric parameters also greatly influence the performance of turbomachinery. Using the control parameters of the meridional plane as design parameters, a mixed-flow pump overall performance have been successfully improved by Suh et al. (2019). By modifying the position of the shroud, the effect of overflow area on the impeller energy characteristics was investigated by Bing et al. (2013). Shim et al. (2018) improved a mixed-flow pump flow recirculation and cavitation performance by modifying the position of the blade inlet, as well as the hub and shroud profile. Si et al. (2020) completed the optimization of an automotive electronic pump with inlet and outlet diameter as design parameters, as well as blade number. Taking the arc radius and angle of the hub and shroud as design parameters, the cooling water pump used in nuclear plants was improved in its operational efficiency by Pei et al. (2016). Overall, it is necessary to take into account the presence of geometrical parameters in the optimized design, as they can effectively affect the turbomachinery's performance.

This work aims to research the impact of hydrodynamic and geometric parameters on mixed-flow pump performance in a bid to improve its performance further. Optimization based on the Taguchi method was adopted to improve the energy characteristics of the impeller by coupling its geometric and hydrodynamic parameters. The parameters' main and secondary effect were then determined by range analysis, and the equations between design parameters and objectives were established by regression variance analysis. Finally, the flow loss visualization technique was employed to clarify the optimization mechanism.

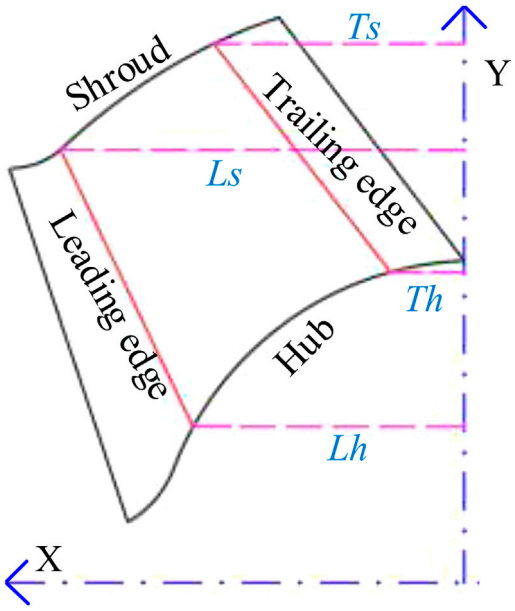

FIGURE 1
Meridional plane of the original model impeller.

TABLE 1 Original model design parameters.

Item	Symbols	Value
Design head	H_d	12.66 m
Design flow rate	Q_d	0.42 m^3/s
Impeller blade number	B	4
Impeller diameter	D	320 mm
Impeller hub radius	R_h	115 mm
Impeller shroud radius	R_s	195.3 mm
Rotating speed	N	1,450 rpm
Specific speed	n_s	511

2 Methodology

2.1 Calculation setup and validation

2.1.1 Original model and geometric parameter definition

The original model chosen for this investigation is a mixed-flow pump used in coastal pumping stations. Figure 1 is the impeller

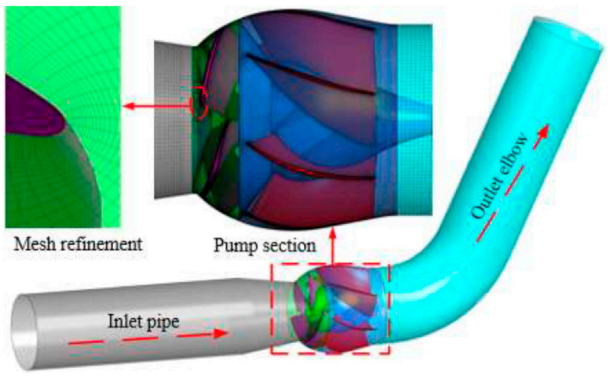

FIGURE 2
Mesh division.

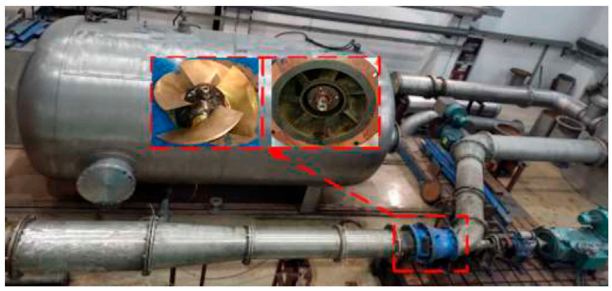

FIGURE 3
Test bench.

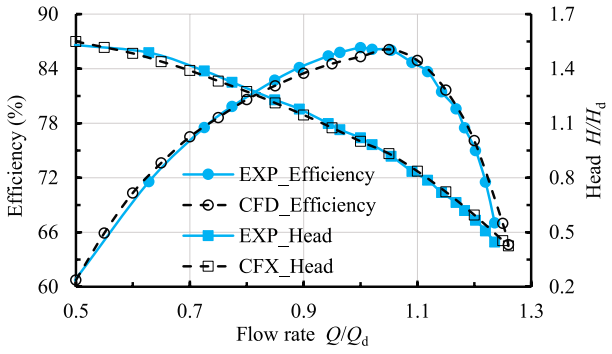

FIGURE 4
Comparison between experimental and predicted performance.

TABLE 2 Mesh-independence analysis results.

Scheme	1	2	3	4	5
Inlet pipe ($\times 10^6$)	0.19	0.43	0.83	1.18	1.67
Impeller ($\times 10^6$)	0.31	0.63	1.40	1.72	2.41
Diffuser ($\times 10^6$)	0.39	0.70	1.42	1.87	2.69
Outlet elbow ($\times 10^6$)	0.41	0.48	0.95	1.33	1.72
Overall ($\times 10^6$)	1.30	2.34	4.60	6.10	8.49
Efficiency (%)	83.72	84.53	85.11	85.12	85.11
Head (m)	12.03	12.13	12.11	12.11	12.11

meridional plane, where the X-axis indicates the rotation axis, and the intersection of the Y-axis and X-axis is the circle center of the shroud and hub profile. *Ls* and *Lh* are the distances from the intersection of the blade leading edge with shroud and hub to the Y-axis, respectively. Similarly, *Ts* and *Th* are the distances from the intersection of the blade trailing edge with shroud and hub to the Y-axis, respectively. Table 1 lists the model's major design parameters.

2.1.2 Original model and geometric parameter definition

A calculation domain (Figure 2), consisting of four components—the output elbow, diffuser, impeller and inlet pipe—was constructed to ensure that the numerical simulation accurately reflects the experimental condition. To improve the computational convergence and accuracy, structured meshes with O-type topology were used to mesh the outlet elbow and inlet pipe in ANSYS-ICEM, and hexahedral structured meshes with H/C-type and O-type topologies were used to mesh the impeller and diffuser in ANSYS-Turbogrid. For the same purpose, all the meshes near the walls were refined.

The mesh-independence analysis results are presented in Table 2. When the number of grids is greater than 4.6 million, the calculated values of head and efficiency almost not change with the number of grids. Therefore, after taking into account the cost and accuracy of the calculation, scheme 3 was adopted for meshing the computational domain in this study, and the maximum Y+ near the wall is 46.

2.1.3 Original model and geometric parameter definition

The commercial software ANSYS-CFX was employed in this study to perform the full-channel numerical simulation of mixed-flow pumps with the help of *k–ω* shear stress transport turbulence model. "Opening" and "Mass flow rate" were employed in the outlet and inlet, respectively. The interface between the rotating and fixing parts is "Frozen rotor". The convective term was discretized by "High resolution". "Automatic wall function" and "No slip wall" were employed for all walls (Menter, 1994; Menter et al., 2003; Hieninger et al., 2021). The number of iterative steps was set to 1,000 and the convergence criterion was set to 10^{-5}.

2.1.4 Experimental verification

A closed test stands at Jiangsu University (Figure 3) with comprehensive uncertainty of 0.28% was used to test the performance of the original model to check the numerical simulation accuracy. The following is the description of the main equipments and their accuracy: EJA intelligent differential pressure transmitters with 0.1% accuracy, JCL1 intelligent torque-speed

sensor with 0.1% accuracy, OPTIFLUX 2000F intelligent electromagnetic flowmeter with 0.2% accuracy, CY200 pressure sensors with 0.1% accuracy.

Figure 4 gives the comparison of the original model prediction results with the experimental results. The predicted performance can be seen highly consistent with the experimental performance in the range of $0.5Q_{des}$ to $1.3Q_{des}$, and the largest error between them does not exceed 2.5%. Hence, it can be considered that the numerical simulation has adequate precision to guarantee the credibility of this study.

2.2 Circulation method and validity verification

2.2.1 Governing equation

The proved circulation method based on the inviscid assumption was adopted to parameterize the blade (Zangeneh et al., 1998). To save space, only a brief description of the core computation was given here; for more details, please refer to the original literature (Zangeneh, 1991). In flow field calculation, velocity was divided into circumferential average and periodic velocity, which can be calculated by the following equations.

$$\frac{\partial}{\partial r}\left(\frac{1}{rB_f}\frac{\partial \varphi}{\partial r}\right)+\frac{\partial}{\partial z}\left(\frac{1}{rB_f}\frac{\partial \varphi}{\partial z}\right)=\frac{\partial r\bar{V}_\theta}{\partial z}\frac{\partial f}{\partial r}-\frac{\partial r\bar{V}_\theta}{\partial r}\frac{\partial f}{\partial z} \tag{1}$$

$$\frac{\partial^2\Phi_m}{\partial r^2}+\frac{1}{r}\frac{\partial\Phi_m}{\partial r}+\frac{\partial^2\Phi_m}{\partial z^2}-\frac{m^2B^2}{r^2}\Phi_m = \frac{e^{-imBf(r,z)}}{imB}\left(\nabla^2 r\overline{V_\theta}\right)-e^{-imBf(r,z)}\left(\frac{\partial f}{\partial r}\frac{\partial r\overline{V_\theta}}{\partial r}+\frac{\partial f}{\partial z}\frac{\partial r\overline{V_\theta}}{\partial z}\right) \tag{2}$$

where φ represents the stream function; Φ_m represents the potential function; z represents the axial coordinate; r represents the radial coordinate; i represents the imaginary unit; i represents the wrap angle; m represents the number of Fourier expansion terms; B represents the blade number; B_f represents the blocking factor; $\overline{V_\theta}$ represents the circumferential-averaged tangential velocity.

The blade shape was calculated by Eq. 3

$$\left(\overline{V_z}+v_z\right)\frac{\partial f}{\partial z}+\left(\overline{V_r}+v_r\right)\frac{\partial f}{\partial r}=\frac{r\overline{V_\theta}}{r^2}+\frac{v_\theta}{r}-\omega \tag{3}$$

where ω represents the angular velocity; v represents the periodic velocity; $\bar{V}$ represents the circumferential-averaged velocity.

2.2.2 Hydrodynamic parameter definition

From the control equation, it is clear that the parameter $r\overline{V_\theta}$ has a decisive influence on the calculation results of the circulation method. Hawthorne et al. (1984) and Nahon et al. (2021) pointed out that $r\overline{V_\theta}$ and blade pressure were related by Eq. 4:

$$\Delta p = p^+ - p^- = \frac{2\pi}{B}W_s\frac{\partial r\overline{V_\theta}}{\partial s} \tag{4}$$

where W_s represents the relative velocity on the meridional plane; p^- represents the suction surface static pressure; p^+ represents the pressure surface static pressure.

Therefore, to facilitate the blade pressure control, blade loading ($\partial r\overline{V_\theta}/\partial s$) at shroud and hub was controlled by the segmented curve in the circulation method (Figure 5), where LE denotes the preloading, ND denotes the second loading point, NC denotes the first loading point, K denotes the straight line slope. It should be noted that only the blade loading at the hub and shroud was controlled by the above segmented curve, while the blade loading at other positions on the meridional plane was obtained by linear interpolation.

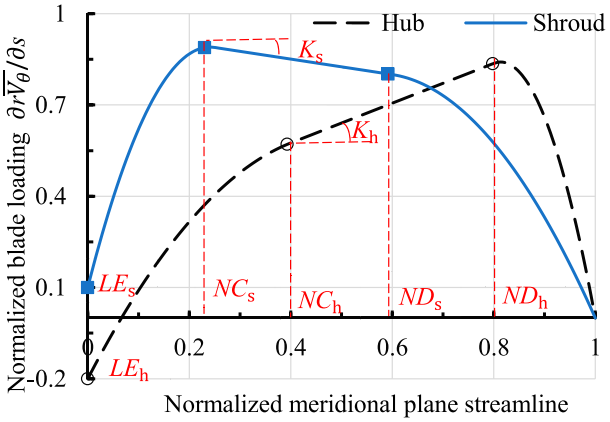

FIGURE 5
Hydrodynamic parameters definition schematic.

3 Optimization design based on Taguchi method

3.1 Optimization targets and test factors

To make the optimized mixed-flow pump have better energy characteristics and similar head, the head and efficiency at $1.0Q_{des}$ were taken as the constraint and optimization target in this study.

The hub ratio was maintained during the optimization process to provide a better match between the diffuser and the optimized impeller (Wang et al., 2021b). Thus, in the parameterization of the impeller, the geometric parameters *Lh*, *Ls*, *Th* and *Ts* shown in Figure 1 were used for the parametrization of the meridional plane, and the hydrodynamic parameters LE_h, NC_h, ND_h, K_h, LE_s, NC_s, ND_s and K_s shown in Figure 5 were used for the blade parametrization. Zhu et al. (2018) indicated that the inclination angle at blade trailing edge (*ST*) has a large influence on the calculation results of the circulation method; therefore, *ST* was also selected as a test factor in this study. To facilitate the subsequent range analysis, the level of each factor was set to 3, as shown in Table 3.

3.2 Experimental scheme and calculation result

Taguchi method (Yang et al., 2021; Bai et al., 2022) has the advantages of reasonable experimental arrangement, short cycle and low cost, making it wise to be used for the experimental scheme construction in this study. From the above analysis, the number of factors and their levels were 13 and 3 respectively, therefore, the L27 (3^{13}) standard orthogonal table was employed for the construction of

TABLE 3 Relationship between the test factors true value and level.

Factors		Geometric parameters					Hydrodynamic parameters							
		Lh/mm	*Ls*/mm	*Th*/mm	*Ts*/mm	*ST*/°	LE_h	NC_h	ND_h	K_h	LE_s	NC_s	ND_s	K_s
Levels	1	85.5	126	14	76	-20	-0.2	0.1	0.5	-1.6	-0.2	0.1	0.5	-1.6
	2	90	133	16	80	0	0	0.3	0.7	0	0	0.3	0.7	0
	3	94.5	140	18	84	20	0.2	0.5	0.9	1.6	0.2	0.5	0.9	1.6

TABLE 4 Experimental scheme and calculation results.

Item no.	Factors													Targets	
	Lh	*Ls*	*Th*	*Ts*	*ST*	LE_h	NC_h	ND_h	K_h	LE_s	NC_s	ND_s	K_s	η/%	*H*/m
1	1	1	1	1	1	1	1	1	1	1	1	1	1	83.43	13.07
2	2	2	2	2	2	1	1	1	1	2	2	2	2	86.69	13.00
3	3	3	3	3	3	1	1	1	1	3	3	3	3	87.96	12.49
4	2	3	3	3	2	2	1	2	2	2	1	1	1	86.86	13.38
5	3	1	1	1	3	2	1	2	2	3	2	2	2	86.57	13.12
6	1	2	2	2	1	2	1	2	2	1	3	3	3	85.98	11.26
7	3	2	2	2	3	3	1	3	3	3	1	1	1	86.52	12.62
8	1	3	3	3	1	3	1	3	3	1	2	2	2	85.51	11.26
9	2	1	1	1	2	3	1	3	3	2	3	3	3	84.59	11.11
10	3	2	1	3	2	3	2	1	2	1	1	2	3	87.07	12.87
11	1	3	2	1	3	3	2	1	2	2	2	3	1	87.62	13.17
12	2	1	3	2	1	3	2	1	2	3	3	1	2	85.91	12.50
13	1	1	3	2	3	1	2	2	3	2	1	2	3	83.86	12.01
14	2	2	1	3	1	1	2	2	3	3	2	3	1	85.81	11.96
15	3	3	2	1	2	1	2	2	3	1	3	1	2	85.54	12.63
16	2	3	2	1	1	2	2	3	1	3	1	2	3	87.69	12.67
17	3	1	3	2	2	2	2	3	1	1	2	3	1	86.27	12.60
18	1	2	1	3	3	2	2	3	1	2	3	1	2	87.37	12.30
19	2	3	1	2	3	2	3	1	3	1	1	3	2	86.65	12.53
20	3	1	2	3	1	2	3	1	3	2	2	1	3	84.81	12.22
21	1	2	3	1	2	2	3	1	3	3	3	2	1	85.96	12.90
22	3	2	3	1	1	3	3	2	1	2	1	3	2	87.50	12.79
23	1	3	1	2	2	3	3	2	1	3	2	1	3	87.08	13.18
24	2	1	2	3	3	3	3	2	1	1	3	2	1	86.52	12.14
25	1	1	2	3	2	1	3	3	2	3	1	3	2	85.01	12.31
26	2	2	3	1	3	1	3	3	2	1	2	1	3	85.52	12.08
27	3	3	1	2	1	1	3	3	2	2	3	2	1	87.18	12.13

the experimental scheme, and a total of 27 different schemes were created.

Table 4 is the factors and targets of each scheme. In contrast to the original model efficiency (85.31%) and head (12.42 m), there were 21 schemes with improved efficiency, 16 schemes with the required head, and 15 schemes with both head and efficiency. Furthermore, scheme 4 has the highest head of 13.38 m, while scheme 3 has the highest efficiency of 87.96%.

TABLE 5 Range analysis results.

Item factors	Efficiency					Head				
	$\overline{K_1}$	$\overline{K_2}$	$\overline{K_3}$	R^*	Rank	$\overline{K_1}$	$\overline{K_2}$	$\overline{K_3}$	R^*	Rank
Lh	85.76	86.25	86.60	0.84	3	12.38	12.37	12.61	0.23	10
Ls	85.22	86.49	86.90	1.68	1	12.34	12.42	12.60	0.26	9
Th	86.19	86.26	86.15	0.11	12	12.47	12.45	12.45	0.03	13
Ts	86.05	86.24	86.32	0.28	9	12.62	12.43	12.33	0.29	8
ST	85.98	86.12	86.51	0.53	6	12.21	12.66	12.50	0.46	4
LE_h	85.67	86.46	86.48	0.81	4	12.41	12.55	12.40	0.15	12
NC_h	86.01	86.35	86.25	0.34	8	12.37	12.52	12.48	0.16	11
ND_h	86.23	86.19	86.18	0.05	13	12.75	12.50	12.12	0.63	1
K_h	86.72	86.41	85.47	1.25	2	12.69	12.54	12.14	0.56	2
LE_s	85.83	86.28	86.50	0.67	5	12.27	12.46	12.64	0.37	7
NC_s	86.07	86.21	86.33	0.27	10	12.69	12.51	12.16	0.53	3
ND_s	85.89	86.34	86.38	0.48	7	12.66	12.46	12.25	0.42	6
K_s	86.24	86.31	86.06	0.24	11	12.66	12.49	12.21	0.45	5

3.3 Range analysis

The influence order of factors on the target, and the trend of the target with the level of factors is defined by extreme analysis (Ahmad and Prakash, 2021). The range R^* was calculated by the following equations:

$$K_i = \sum_{j=1}^{9} Y_{ij} \tag{5}$$

$$\overline{K_i} = \frac{K_i}{9} \tag{6}$$

$$R^* = \max\left(\bar{K}_1, \bar{K}_2, \bar{K}_3\right) - \min\left(\bar{K}_1, \bar{K}_2, \bar{K}_3\right) \tag{7}$$

where i is the level; Y_{ij} is the target value of a factor with level i; K_i is the sum of the Y_{ij}.

Table 5 is the efficiency and head range analysis results. The effect order of factors on efficiency is *Ls*, K_h, *Lh*, LE_h, LE_s, *ST*, ND_s, NC_h, T_s, NC_s, K_s, *Th* and ND_h, while the effect order of factors on head is ND_h, *Kh*, NC_s, *ST*, K_s, ND_s, LE_s, *Ts*, *Ls*, *Lh*, NC_h, LE_h and *Th*. Therefore, both hydrodynamic and geometric parameters should be considered simultaneously in the mixed-flow pump optimization design to maximize the energy characteristics improvement, since both of them have a large influence on the efficiency. To show the trend of the target with the level of factors more intuitively, geometric and hydrodynamic parameters' main effects on the target were plotted in Figure 6 according to Table 5.

3.4 Regression analysis of variance

To obtain the response relationship between the factors and the objectives, the data in Table 4 were subjected to a regression analysis of variance (Chiranjeevi et al., 2022). It is generally accepted that the correlation between the test factors and the optimization objectives is statistically significant when the p-value is less than 0.05. Therefore, according to the results of variance analysis in Table 6, parameters *Ls*, K_h, *Lh*, LE_h and LE_s were significant factors for efficiency, and parameters ND_h, K_h, NC_s, K_s, ND_s and LE_s were significant factors for head. The results of the p-value analysis once again show that both the geometric and hydrodynamic parameters have significant influence on the mixed-flow pump energy characteristics. Equation 8 and Equation 9 are the efficiency and head regression equations, respectively.

$$\begin{aligned}\eta_D = {} & 81.924 + 0.422Lh + 0.840Ls - 0.022Th + 0.139Ts + 0.265ST \\ & + 0.407LE_h + 0.118NC_h - 0.024ND_h - 0.626K_h + 0.334LE_s \\ & + 0.134NC_s + 0.242ND_s - 0.089K_s\end{aligned} \tag{8}$$

$$\begin{aligned}H_D = {} & 14.118 + 0.112Lh + 0.131Ls - 0.014Th - 0.145Ts + 0.144ST \\ & - 0.002LE_h + 0.054NC_h - 0.315ND_h - 0.278K_h - 0.278K_h \\ & + 0.184LE_s - 0.266NC_s - 0.209ND_s - 0.227K_s\end{aligned} \tag{9}$$

3.5 Optimal model determination and performance comparison

To make the optimized mixed-flow pump with better energy characteristics and suitable head, the levels of the test factors *Lh*, *Ls*, *Th*, *Ts*, *ST*, LE_h, NC_h, ND_h, K_h, LE_s, NC_s, ND_s and K_s were set to 3, 3, 2, 3, 3, 3, 2, 1, 1, 3, 3, 3 and 2, respectively, based on the results of the range and regression analyses.

Figure 7 shows the impeller shape comparison between the original and optimized model. Compared to the original model

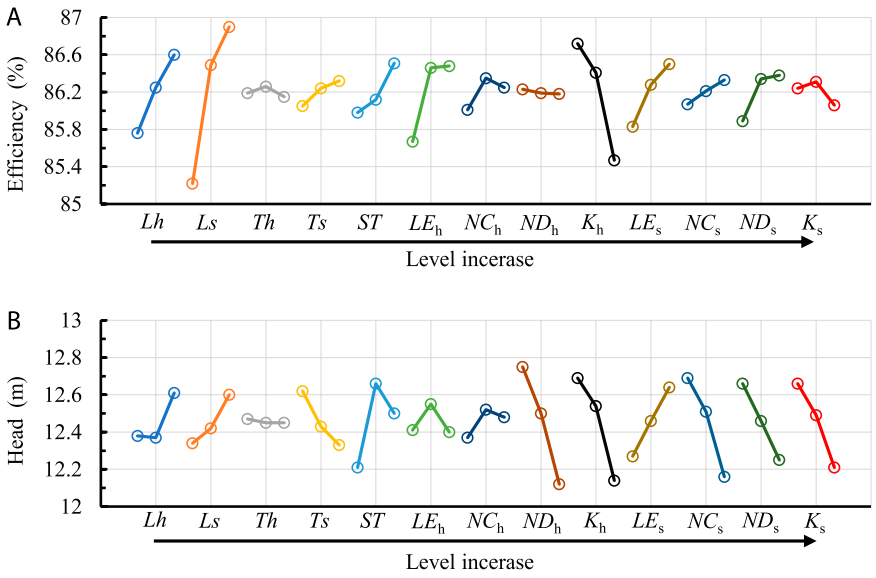

FIGURE 6
Main effect of hydrodynamic and geometric parameters on the objectives: **(A)** Efficiency; **(B)** Head.

TABLE 6 Results of the variance regression analysis.

Source	Freedom degree	Efficiency				Head			
		Adj SS	Adj SS	F- value	*p*-value	Adj SS	Adj SS	F- value	*p*-value
Regression	13	31.345	2.411	8.781	0.000	8.112	0.624	7.598	0.000
Lh	1	3.209	3.209	11.687	0.005	0.224	0.224	2.733	0.122
Ls	1	12.701	12.701	46.255	0.000	0.309	0.309	3.767	0.074
Th	1	0.009	0.009	0.032	0.860	0.004	0.004	0.046	0.834
Ts	1	0.347	0.347	1.265	0.281	0.378	0.378	4.608	0.051
ST	1	1.264	1.264	4.604	0.051	0.376	0.376	4.572	0.052
LE_h	1	2.977	2.977	10.841	0.006	0.000	0.000	0.001	0.974
NC_h	1	0.250	0.250	0.909	0.358	0.052	0.052	0.636	0.439
ND_h	1	0.011	0.011	0.039	0.846	1.786	1.786	21.745	0.000
K_h	1	7.044	7.044	25.653	0.000	1.389	1.389	16.910	0.001
LE_s	1	2.013	2.013	7.332	0.018	0.609	0.609	7.411	0.017
NC_s	1	0.325	0.325	1.185	0.296	1.275	1.275	15.519	0.002
ND_s	1	1.051	1.051	3.829	0.072	0.785	0.785	9.562	0.009
K_s	1	0.144	0.144	0.524	0.482	0.925	0.925	11.259	0.005
Error	13	3.570	0.275			1.068	0.082		
Total	26	34.914				9.180			

the optimized model has an increased overflow area at the hub and a reduced overflow area at the shroud. In addition, the optimized model blade trailing edge inclination angle is also increased. Figure 8 is the energy characteristics comparison between the optimized and original model. The optimized model efficiency and head at design condition are 88.51% and 12.43 m respectively, representing a 3.2% increase in efficiency and almost no change in head. The improved efficiency and nearly unchanged head indicate that the geometric and hydrodynamic parameters adopted in this study are reasonable.

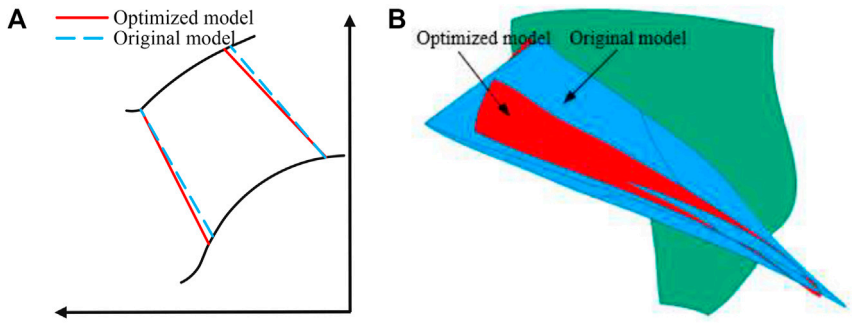

FIGURE 7
Comparison of original and optimized model impeller shapes: **(A)** Meridional plane; **(B)** blade shape.

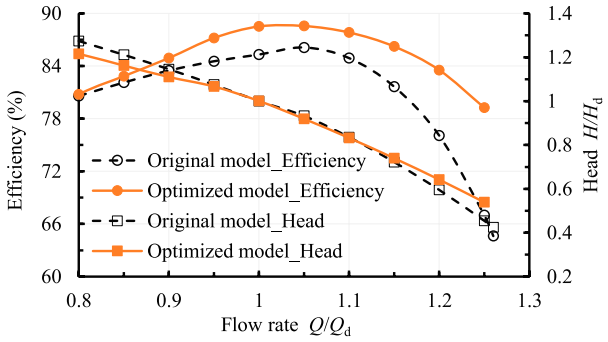

FIGURE 8
Comparison of original and optimized model energy characteristic.

4 Energy loss analysis

4.1 Entropy production theory

To elucidate the optimization mechanism, the energy loss of the optimized model was comparatively analyzed with that of the original model using entropy production theory. Similarly, only a brief introduction to the main computational equations of entropy production theory was given here; for more details, please refer to the original literature (Kock and Herwing, 2004; Qi et al., 2022).

For turbulent flow of viscous fluids, the entropy is largely induced by viscous dissipation, turbulent kinetic energy dissipation and wall effects, and are respectively calculated using the following equations.

$$E_V = \frac{\mu}{T}\left\{2\left[\left(\frac{\partial \bar{u}}{\partial x}\right)^2 + \left(\frac{\partial \bar{v}}{\partial y}\right)^2 + \left(\frac{\partial \bar{w}}{\partial z}\right)^2\right] + \left(\frac{\partial \bar{u}}{\partial y} + \frac{\partial \bar{v}}{\partial x}\right)^2 + \left(\frac{\partial \bar{v}}{\partial z} + \frac{\partial \bar{w}}{\partial y}\right)^2 + \left(\frac{\partial \bar{u}}{\partial z} + \frac{\partial \bar{w}}{\partial x}\right)^2\right\} \tag{10}$$

$$E_T = 0.09\frac{\rho\varepsilon}{T} \tag{11}$$

$$E_W = \frac{\vec{\tau}\cdot\vec{v}}{T} \tag{12}$$

where E_V represents the viscous dissipation induced direct entropy production rate; E_T represents the turbulent kinetic energy dissipation induced indirect entropy production rate; E_W represents the wall effects induced wall entropy production rate; ρ represents fluid density; ε represents the turbulent dissipation rate; T represents the thermodynamic temperature; $\vec{v}$ represents the first grid node velocity; $\vec{\tau}$ represents the shear stress; μ represents the dynamic viscosity; u, v and w represent the flow velocity components of x, y and z axis, respectively.

ΔE is calculated by the following equation:

$$\Delta E = \Delta E_V + \Delta E_T + \Delta E_w = T\left(\int_V E_V dV + \int_V E_T dV + \int_S E_W dS\right) \tag{13}$$

where ΔE, ΔE_V, ΔE_T and ΔE_w represent the total, direct, indirect and wall entropy production, respectively.

4.2 Analysis of energy loss

The comparison of different types of entropy production distributions for the optimized and original models can be found in Figure 9. The total entropy production of the optimized model was significantly reduced in comparison to the original model, especially in the impeller, diffuser and outlet pipe, where total entropy production was reduced by 104.31, 389.66 and 308.61 W, respectively. When specific to the different types of entropy production, the variation of total entropy production in the impeller was mainly caused by both indirect and wall entropy production, while the variation of total entropy production in the diffuser and outlet pipe was mainly induced by indirect entropy production.

To better clarify how the mixed flow pump's energy loss characteristics are affected by internal flow patterns, the energy dissipation caused by the fluid motion was defined as the fluid entropy production rate (FEPR), whose value is equal to the sum of the direct and indirect entropy production rate.

The distribution of FEPR for the optimized and original models at impeller different spans is shown in Figure 10. The optimized and

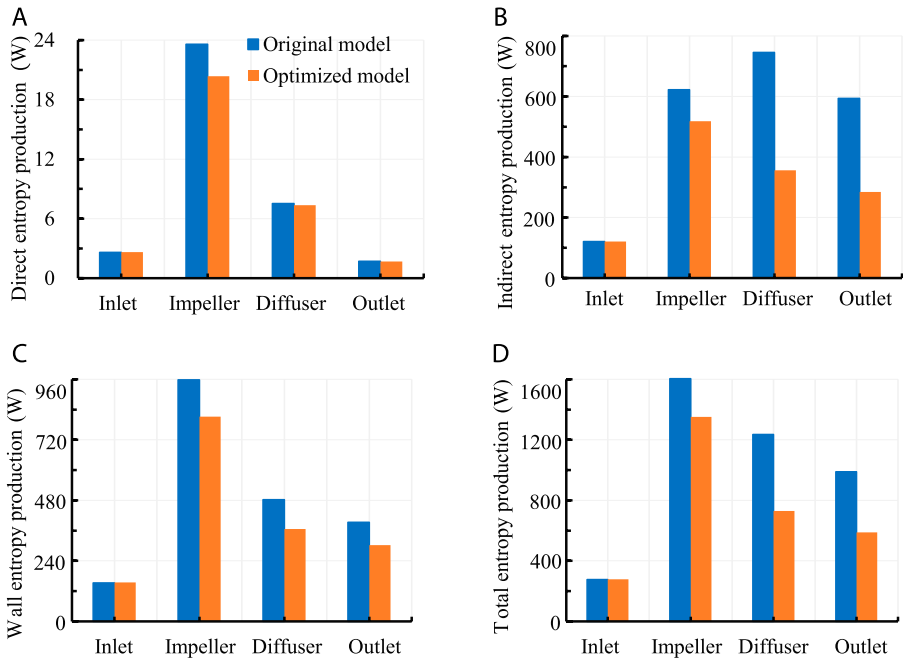

FIGURE 9
Comparison of different types of entropy production distribution: **(A)** ΔE_V; **(B)** ΔE_T; **(C)** ΔE_w; **(D)** ΔE.

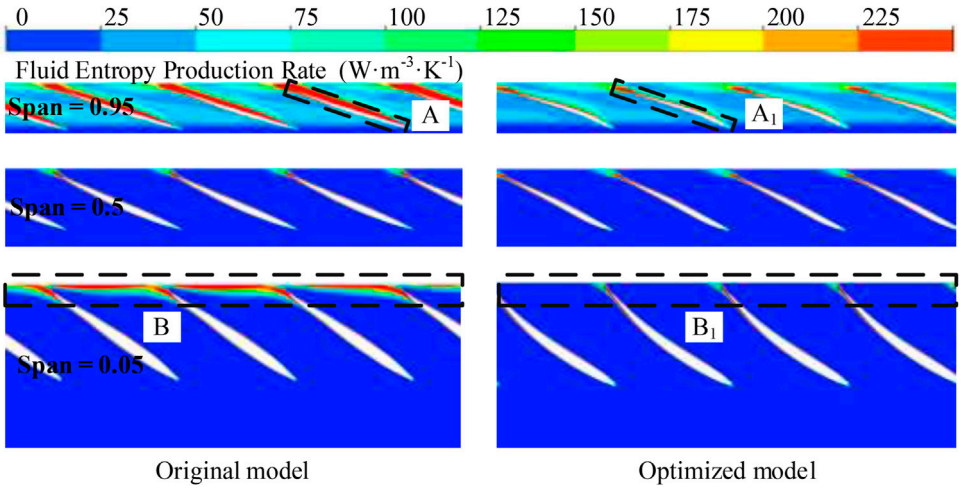

FIGURE 10
Impeller FEPR distribution comparison.

original model mid-span FEPR distribution was basically the same, and a larger FEPR caused by the jet-wake (Wu et al., 2021) was observed at blade trailing edge. However, compared to the original model, the FEPR in the optimized model shroud was markedly decreased, especially near the pressure surface. Also, near the hub of the impeller, the FEPR of the optimized model at the blade trailing edge was markedly decreased compared to the original model.

Although the diffuser is the same for the optimized and original models, the FEPR distribution in the two diffusers is quite different due to the difference of impeller outlet flow regime. Figures 11, 12 are the impeller outlet axial velocity distribution and diffuser different spans FEPR distribution respectively. The axial velocity at the outlet of the original model impeller increases progressively from the hub to shroud, and backflow was generated in a small region near the hub due to the boundary layer detachment

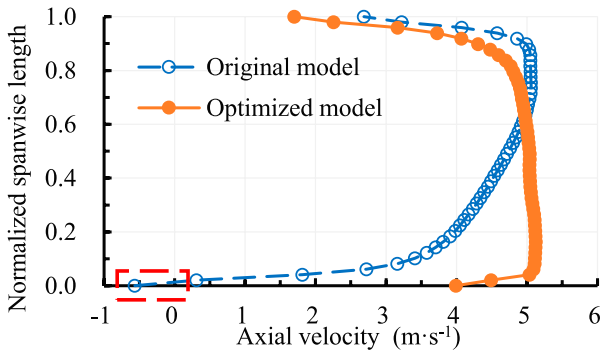

FIGURE 11
Impeller outlet axial velocity distribution comparison.

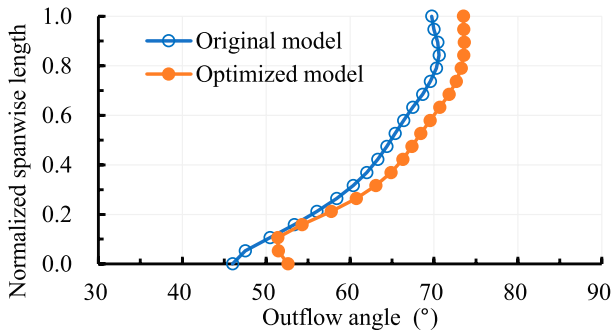

FIGURE 13
Diffuser outlet outflow angle distribution comparison.

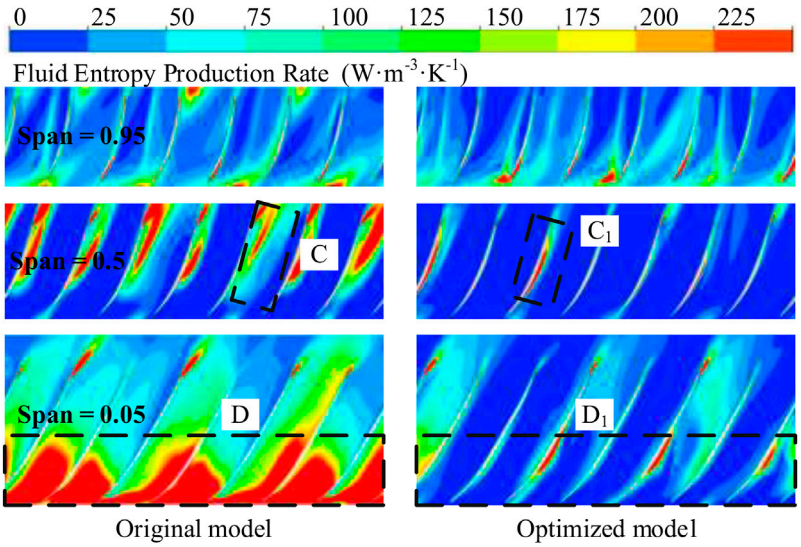

FIGURE 12
Diffuser FEPR distribution comparison.

(Kim et al., 2020). Due to the adverse flow pattern at the outlet of the original model impeller, a large FEPR was produced near the hub at the inlet of the diffuser, as shown in region D of Figure 12. After optimization, the axial velocity at impeller outlet near the hub was significantly increased, which effectively prevents the boundary layer detachment caused by the accumulation of low-momentum fluid. Accordingly, the FEPR near the hub at the inlet of the diffuser is markedly reduced.

A similar analysis was performed on the outlet pipe. Figure 13 is the distribution of the outflow angle θ at the diffuser outlet, which is calculated by Eq. 14. The optimized model has a larger outflow angle throughout the diffuser outlet than the original model, which means that the fluid residual rotational kinetic energy at the diffuser outlet is smaller for the optimized model. Lu et al. (2018) indicated that the fluid residual rotational kinetic energy at diffuser outlet is the outlet pipe energy loss primary

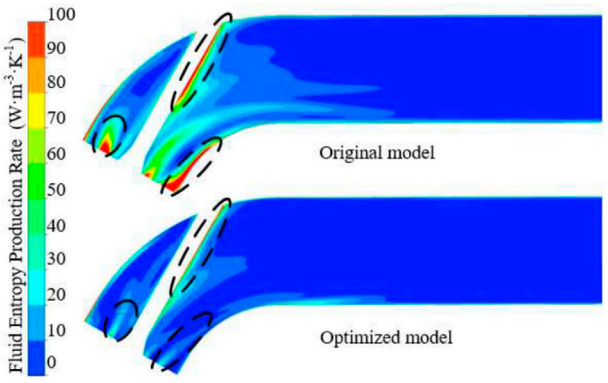

FIGURE 14
Outlet pipe FEPR distribution comparison.

cause. Therefore, the optimized model outflow pipe FEPR was remarkably lower than that of the original model, as shown in Figure 14.

$$\theta = \arcsin\frac{V_Z}{V} \tag{14}$$

where V represent the velocity, V_Z represent the z-axial component of velocity.

5 Conclusion

In this work, a typical mixed-flow pump was numerically simulated and experimentally verified. Then, its impeller was parameterized by five geometric and eight hydrodynamic parameters and optimized using the Taguchi method. Finally, the main and minor order of the parameters were determined using range and regression analysis, and the optimization mechanism was revealed by the energy loss visualization technique. The following conclusions were drawn:

(1) The geometric parameters *Ls* and *Lh*, as well as the hydrodynamic parameters LE_h, LE_s and K_h have a great influence on the mixed-flow pump efficiency. To maximize the energy characteristics of the mixed-flow pump, both geometric and hydrodynamic parameters need to be considered in its optimization design.
(2) The efficiency and head of the optimized model at the design condition are 88.51% and 12.43 m respectively, which represents a 3.2% increase in efficiency and almost no change in head compared to the original model. The improved efficiency and nearly unchanged head indicate that the geometric and hydrodynamic parameters adopted in this study are reasonable.
(3) The reduction of energy loss in the impeller downstream components induced by the improved flow pattern at impeller outlet contributes more than 87% to the performance improvement. Therefore, in the optimization of mixed-flow pump impeller, not only the improvement of impeller energy characteristics should be concerned, but also the change of its outlet flow pattern.

Data availability statement

The original contributions presented in the study are included in the article/supplementary material, further inquiries can be directed to the corresponding author.

Author contributions

JC: Writing–original draft, Software, Methodology. YB: Writing–review and editing. MW: Supervision, Guidance. HX: Supervision. XC: Data curation.

Conflict of interest

Author XC was employed by Anhui Ding Yuan Engineering Construction Co., HX was employed by Jiangsu Province Water Engineering Sci-tech Consulting Co.

The remaining author declares that the research was conducted in the absence of any commercial or financial relationships that could be construed as a potential conflict of interest.

Publisher's note

All claims expressed in this article are solely those of the authors and do not necessarily represent those of their affiliated organizations, or those of the publisher, the editors and the reviewers. Any product that may be evaluated in this article, or claim that may be made by its manufacturer, is not guaranteed or endorsed by the publisher.

References

Ahmad, S., and Prakash, O. (2021). Optimization of ground heat exchanger of the ground source heat pump system based on exergetic analysis using Taguchi technique. *P I Mech. Eng. C-J Mec.* 235 (21), 5892–5901. doi:10.1177/0954406221991183

Bai, L., Yang, Y., Zhou, L., Li, Y., Xiao, Y., and Shi, W. (2022). Optimal design and performance improvement of an electric submersible pump impeller based on Taguchi approach. *Energy* 252, 124032. doi:10.1016/j.energy.2022.124032

Bing, H., Cao, S., Tan, L., and Zhu, B. (2013). Effects of meridional flow passage shape on hydraulic performance of mixed-flow pump impellers. *Chin. J. Mech. Eng-en* 26 (3), 469–475. doi:10.3901/cjme.2013.03.469

Bonaiuti, D., Zangeneh, M., Aartojarvi, R., and Eriksson, J. (2010). Parametric design of a waterjet pump by means of inverse design, CFD calculations and experimental analyses. *J. Fluid Eng-T Asme* 132 (3), 031104. doi:10.1115/1.4001005

Bonaiuti, D., and Zangeneh, M. (2009). On the coupling of inverse design and optimization techniques for the multiobjective, multipoint design of turbomachinery blades. *J. Turbomach.* 131 (2), 021014. doi:10.1115/1.2950065

Chiranjeevi, P., Ashok, V., Srinivasan, K., and Sundararajan, T. (2022). Performance analysis of single-phase space thermal radiators and optimization through taguchi-neuro-genetic approach. *J. Therm. Sci. Eng. Appl.* 14 (6), 061012. doi:10.1115/1.4052897

Fallah-Ardeshir, H., Ehghaghi, B., and Nill-Ahmadabadi, M. (2020). Inverse design of a centrifugal pump on the meridional plane using ball-spine algorithm. *Sci. Iran.* 27 (5), 2478–2488.

Goto, A., Takemura, T., and Zangeneh, M. (1996). Suppression of secondary flows in a mixed-flow pump impeller by application of three-dimensional inverse design method: Part 2-experimental validation. *J. Turbomach.* 118 (3), 544–551. doi:10.1115/1.2836701

Gu, Y., Cheng, J., Wang, P., Cheng, L., Si, Q., Wang, C., et al. (2022). A flow model for side chambers of centrifugal pumps considering radial wall shear stress. *P I Mech. Eng. C-J Mec.* 236 (13), 7115–7126. doi:10.1177/09544062211073023

Gu, Y., Li, J., Wang, P., Cheng, L., Qiu, Y., Wang, C., et al. (2022). An Improved one-dimensional flow model for side chambers of centrifugal pumps considering the blade slip factor. *J. Fluid Eng-T Asme* 144 (9), 091207. doi:10.1115/1.4054138

Hawthorne, W., Wang, C., and McCune, J. (1984). Theory of blade design for large deflections: Part I-two-dimensional cascade. *J. Eng. Gas. Turb Power* 106 (2), 346–353. doi:10.1115/1.3239571

Hieninger, T., Schmidt-Vollus, R., and Schlucker, E. (2021). Improving energy efficiency of individual centrifugal pump systems using model-free and on-line optimization methods. *Appl. Energ* 304, 117311. doi:10.1016/j.apenergy.2021.117311

Huang, R., Luo, X., Ji, B., Wang, P., Yu, A., Zhai, Z., et al. (2015). Multi-objective optimization of a mixed-flow pump impeller using modified NSGA-II algorithm. *Sci. China Technol. S. C.* 58 (12), 2122–2130. doi:10.1007/s11431-015-5865-5

Kim, S., Kim, Y., Kim, J., and Choi, Y. (2020). Design optimization for mixed-flow pump impeller by improved suction performance and efficiency with variables of specific speeds. *J. Mech. Sci. Technol.* 34 (6), 2377–2389. doi:10.1007/s12206-020-0515-7

Kim, S., Kim, Y., Kim, J., and Choi, Y. (2019). Three-objective optimization of a mixed-flow pump impeller for improved suction performance and efficiency. *Adv. Mech. Eng.* 11 (12), 168781401989896. doi:10.1177/1687814019898969

Kock, F., and Herwing, H. (2004). Local entropy production in turbulent shear flows: A high-Reynolds number model with wall functions. *Int. J. Heat. Mass Tran* 47 (10), 2205–2215. doi:10.1016/j.ijheatmasstransfer.2003.11.025

Lee, K., Choi, Y., Kim, Y., and Yun, J. (2008). Design of axial fan using inverse design method. *J. Mech. Sci. Technol.* 22 (10), 1883–1888. doi:10.1007/s12206-008-0727-8

Leguizamon, S., and Avellan, F. (2020). Open-Source implementation and validation of a 3D inverse design method for Francis turbine runners. *Energies* 13 (8), 2020. doi:10.3390/en13082020

Liang, J., Lu, L., Xu, L., Chen, W., and Wang, G. (2012). Influence of flow velocity circulation at guide vane outlet of axial-flow pump on hydraulic loss in outlet condition. *CSAE* 28 (01), 55–60.

Lu, Y., Wang, X., Wang, W., and Zhou, F. (2018). Application of the modified inverse design method in the optimization of the runner blade of a mixed-flow pump. *Chin. J. Mech. Eng-en* 31 (1), 105. doi:10.1186/s10033-018-0302-x

Ma, Z., Zhu, B., Rao, C., and Shangguan, Y. (2019). Comprehensive hydraulic improvement and parametric analysis of a Francis turbine runner. *Energies* 12 (2), 307. doi:10.3390/en12020307

Menter, F., Ferreira, J., and Esch, T. (2003). *The SST turbulence model with improved wall treatment for heat transfer predictions in gas turbines*. Tokyo, Japan: International Gas Turbine Congress.

Menter, F. (1994). Two-equation eddy-viscosity turbulence models for engineering applications. *AIAA J.* 32 (8), 1598–1605. doi:10.2514/3.12149

Nahon, J., Zangeneh, M., Nohmi, M., Watanabe, H., and Goto, A. (2021). A robust inverse design solver for controlling the potential aggressiveness of cavitating flow on hydrofoil cascades. *Int. J. Numer. Meth Fl* 93 (7), 2291–2310. doi:10.1002/fld.4974

Pei, J., Wang, W., and Yuan, S. (2016). Multi-point optimization on meridional shape of a centrifugal pump impeller for performance improvement. *J. Mech. Sci. Technol.* 30 (11), 4949–4960. doi:10.1007/s12206-016-1015-7

Qi, B., Zhang, D., Geng, L., Zhao, R., and Van Esch. (2022). Numerical and experimental investigations on inflow loss in the energy recovery turbines with back-curved and front-curved impeller based on the entropy generation theory. *Energy* 239 (E), 122426. doi:10.1016/j.energy.2021.122426

Shim, H., Kim, K., and Choi, Y. (2018). Three-objective optimization of a centrifugal pump to reduce flow recirculation and cavitation. *J. Fluid Eng-T Asme* 140 (9), 091202. doi:10.1115/1.4039511

Si, Q., Lu, R., Shen, C., Xia, S., Sheng, G., and Yuan, J. (2020). An intelligent CFD-based optimization system for fluid machinery: Automotive electronic pump case application. *Appl. Sci-basel* 10 (1), 366. doi:10.3390/app10010366

Suh, J., Yang, H., Kim, Y., Lee, K., Kim, J., Joo, W., et al. (2019). Multi-objective optimization of a high efficiency and suction performance for mixed-flow pump impeller. *Eng. Appl. Comp. Fluid* 13 (1), 744–762. doi:10.1080/19942060.2019.1643408

Wang, M., Li, Y., Yuan, J., and Osman, F. (2021). Influence of spanwise distribution of impeller exit circulation on optimization results of mixed flow pump. *Appl. Sci-basel* 11 (2), 507. doi:10.3390/app11020507

Wang, M., Li, Y., Yuan, J., and Osman, F. (2021). Matching optimization of a mixed flow pump impeller and diffuser based on the inverse design method. *Processes* 9 (2), 260. doi:10.3390/pr9020260

Wang, M., Li, Y., Yuan, J., and Yuan, S. (2022). Effects of different vortex designs on optimization results of mixed-flow pump. *Eng. Appl. Comp. Fluid* 16 (1), 36–57. doi:10.1080/19942060.2021.2006091

Wu, C., Li, Q., Zheng, F., Wu, P., Yang, S., Ye, H., et al. (2021). Improve of unsteady pressure pulsation based on jet-wake suppression for a low specific centrifugal pump. *J. Fluid Eng-T Asme* 143 (11), 111202. doi:10.1115/1.4051402

Yang, W., Lei, X., Zhang, Z., Li, H., and Wang, F. (2017). Hydraulic design of submersible axial-flow pump based on blade loading distributions. *CSAM* 48 (11), 179–187.

Yang, W., and Xiao, R. F. (2014). Multiobjective optimization design of a pump-turbine impeller based on an inverse design using a combination optimization strategy. *J. Fluid Eng-T Asme* 136 (1), 014501. doi:10.1115/1.4025454

Yang, Y., Zhou, L., Hang, J., Du, D., Shi, W., and He, Z. (2021). Energy characteristics and optimal design of diffuser meridian in an electrical submersible pump. *Renew. Energ* 167, 718–727. doi:10.1016/j.renene.2020.11.143

Yin, J., and Wang, D. (2014). Review on applications of 3D inverse design method for pump. *Chin. J. Mech. Eng-en* 27 (3), 520–527. doi:10.3901/cjme.2014.03.520

Zangeneh, M. (1991). A compressible three-dimensional design method for radial and mixed flow turbomachinery blades. *Int. J. Numer. Meth Fl* 13, 599–624. doi:10.1002/fld.1650130505

Zangeneh, M., Gota, A., and Takemura, T. (1996). Suppression of secondary flows in a mixed-flow pump impeller by application of three-dimensional inverse design method: Part 1-design and numerical validation. *J. Turbomach.* 118 (3), 536–543. doi:10.1115/1.2836700

Zangeneh, M., Goto, A., and Harada, H. (1998). On the design criteria for suppression of secondary flows in centrifugal and mixed flow impellers. *J. Turbomach.* 120 (4), 723–735. doi:10.1115/1.2841783

Zhang, R., and Zhao, X. (2020). Inverse method of centrifugal pump blade based on Gaussian process regression. *Math. Probl. Eng.* 2020, 1–10. doi:10.1155/2020/4605625

Zhu, B., Tan, L., Wang, X., and Ma, Z. (2018). Investigation on flow characteristics of pump-turbine runners with large blade lean. *J. Fluid Eng-T Asme* 140 (3), 031101. doi:10.1115/1.4037787